prediction of the viability of thiohydroxycarbene. It is clear that the energetic dispositions of the stationary points on the S_0 potential energy surface of thioformaldehyde are in many instances similar to those on the ground-state surface of formaldehyde. Theory suggests[22] that the activation energy for $H_2CO \rightarrow H_2 + CO$ is about 80 kcal/mol, while that for isomerization to hydroxycarbene is about 81 kcal/mol. Clearly the much lower excitation energy for the $^1A_2(S_1)$ state of H_2CS compared to that of H_2CO (80.6 kcal/mol) accounts for the failure to observe photodissociation as an important decay process for H_2CS in its first excited singlet state. As noted previously, this is consistent with LPE[42] and LOAD[36] spectra, where strong emission from highly excited vibrational levels of the A^1A_2 state is observed, in marked contrast to formaldehyde, where dissociation processes become increasingly dominant with increasing energy, resulting in a breakoff in the fluorescence excitation spectrum.

Our best computed estimates of the barrier for dissociation of H_2CS ($^3A''$) to H + HCS ($^2A'$) and for isomerization to HCSH (^3A) on the T_1 surface are 50.4 and 45.7 kcal/mol, respectively, with the ^3A HCSH excited state lying 15.4 kcal/mol above the $^1A'$ state of *trans*-HCSH.

Calculations on the potential energy surface of the thioformaldehyde cation predict H_2CS^+ ($^2B_2$) to be 30.2 kcal/mol more stable than *trans*-$HCSH^+$ ($^2A'$), in good agreement with the separation deduced from photoionization mass spectrometric measurements.[60] A barrier of 55.4 kcal/mol is computed for the rearrangement of H_2CS^+ to the less stable isomer.

The study of the potential energy surface of the thioformyl radical suggests that the HSC → HCS ($^2A'$) isomerization occurs via a two-step mechanism, involving dissociation of HSC and recombination to form the more stable isomer. The corresponding 1,2 hydrogen shift in the thioformyl cation is predicted to occur without activation energy.

Registry No. H_2CS, 865-36-1; H_2DS^+·, 61356-81-8; HCS·, 36058-28-3; HCS^+, 59348-25-3.

Theoretical Determination of Molecular Structure and Conformation. 15. Three-Membered Rings: Bent Bonds, Ring Strain, and Surface Delocalization

Dieter Cremer* and Elfi Kraka

Contribution from the Lehrstuhl für Theoretische Chemie, Universität Köln, D-5000 Köln 41, West Germany. *Received October 10, 1984*

Abstract: Energy, geometry, one-electron density distribution, and Laplace concentrations of cyclopropane (**1**), aziridine (**2**), oxirane (**3**), cyclopropyl anion (**4**), protonated aziridine (**5**), protonated oxirane (**6**), halogen-bridged fluoroethyl cation (**7**), and hydrogen-bridged ethyl cation (**8**) are investigated and compared with their corresponding alicyclic counterparts. The relationship between three-membered rings (3MR) and π-complexes is demonstrated by analyzing their electron density pattern with the aid of catastrophe theory. A continuous change from 3MRs to π-complexes can be observed if the acceptor (donor) ability of a group X interacting with an ethylene unit is increased (decreased). The bend of the 3MR bonds is described by the curvature of the paths of maximum electron density linking the ring atoms. Interpath angles are used to evaluate the strain energy of a 3MR. A value of 75 kcal/mol is found for **1**. Strain is partially compensated by stabilizing effects arising from surface delocalization of σ-electrons of the 3MR (48 kcal/mol for **1**). Both ring strain and surface delocalization increase in the series **1**, **2**, **3** with a slight dominance of the former effect. The chemical relevance of theoretical results is discussed with regard to the ability of 3MRs to interact with π-systems and to undergo addition reactions with electrophiles and nucleophiles. The observed regioselectivity in ring-opening reactions of oxiranes is explained.

I. Introduction

The peculiar properties of three-membered rings (3MR), in particular their ability to interact with π-systems and to stabilize carbenium ions, have intrigued experimentalists and theoreticians for many decades as is amply documented in the literature.[1] In order to rationalize experimental observations on 3MRs, the bonding of cyclopropane (**1**) has been interrelated with that of ethylene, on both the basis of the bent bond description advocated by Coulson and Moffit[2] and the Walsh model of **1**.[3] The bent bond model is often used to analyze energetics (strain)[4] and electron density distribution of 3MRs[5] while the Walsh model is more convenient for analyzing electronic interactions of 3MRs with attached substituents or an annelated ring system.[6] In principle, there is, however, no difference between the two models. They just provide complementary pictures of 3MRs with two different sets of basis orbitals, which are related by a unitary transformation.[7] Taking this into account, it should be possible

(1) (a) Charton, M. "Olefinic Properties of Cyclopropanes" In "The Chemistry of Alkenes"; Zabicky, J., Ed.; Wiley-Interscience: New York, 1970; Vol. 2. (b) Meijere, A. de, *Angew. Chem.* **1979**, *91*, 867-884; *Angew. Chem., Int. Ed. Engl.* **1979**, *18*, 809-826. (c) Gleiter, R. *Top. Curr. Chem.* **1979**, *86*, 197-285. (d) Lathan, W. A.; Random, L.; Hariharan, P. C.; Hehre, W. J.; Pople, J. A. *Top. Curr. Chem.* **1973**, *40*, 1-45. (e) Newton, M. D. In "Modern Theoretical Chemistry"; Schaefer, H. F., Ed.; Plenum Press: New York, 1977; Vol. 4, pp 223-275.

(2) Coulson, C. A.; Moffitt, W. E. *Philos. Mag.* **1949**, *40*, 1-35.

(3) Walsh, A. D. *Trans. Faraday Soc.* **1949**, *45*, 179-190.

(4) (a) Wendisch, D. In "Methoden der Organischen Chemie"; Houben-Weyl-Müller, E.; Thieme Verlag: Stuttgart, 1971; Vol. IV, 3, pp 17-27. (b) Liebman, J. F.; Greenberg, A. *Chem. Rev.* **1976**, *76*, 311-365.

(5) (a) Fritchie, C. J., Jr. *Acta Crystallogr.* **1966**, *20*, 27-36. (b) Hartman, A.; Hirshfeld, F. L. *Acta Crystallogr.* **1966**, *20*, 80-82. (c) Ito, T.; Sakurai, T. *Acta Crystallogr., Sect. B* **1973**, *B29*, 1594-1603. (d) Matthews, D. A.; Stucky, G. D. *J. Am. Chem. Soc.* **1971**, *93*, 5954-5959.

(6) (a) Hoffmann, R. *Tetrahedron Lett.* **1970**, 2907-2909. (b) Günther, H. *Tetrahedron Lett.* **1970**, 5173-5176. (c) Hoffmann, R.; Stohrer, W.-D. *J. Am. Chem. Soc.* **1971**, *93*, 6941-6948. (d) Jorgensen, W. L. *J. Am. Chem. Soc.* **1975**, *97*, 3082-3090.

(7) As has recently been shown, this is not longer valid considering only the bonding basis orbitals: Honegger, E.; Heilbronner E.; Schmelzer, A. *Nouv. J. Chim.* **1982**, *6*, 519-526.

0002-7863/85/1507-3800$01.50/0

Table I. Calculated Energies and Geometries for 3MRs **1–8** and Reference Compounds **10–16**[a]

	energies[b]			geometries[b]			
	C/HF	C/MP	$\Delta H_f°(298)$[d]	*R*(CX)	*R*(CC)	∠CC(HH)	∠(CC)XH
1, X = CH_2	−117.05887	−117.46275	12.7	1.497		150.0	123.0
2, X = NH[c]	−133.03855	−133.47232	30.2	1.449	1.470	154.2	115.4
3, X = O	−152.86736	−153.31513	−12.6	1.401	1.453	158.5	
4 X = CH^-	−116.34943	−116.75688		1.526	1.505	143.5	110.4
5, X = NH_2^+[c]	−133.40780	−133.83337	177.3	1.488	1.460	160.0	121.9
6, X = OH^+[c]	−153.17647	−153.61418	169.6	1.498	1.446	165.5	119.5
7, X = F^+	−177.12564	−177.54941		1.533	1.445	171.3	
8, X = H^+	−78.30994	−78.55991		1.306	1.371	178.3	
	C/HF	C/MP	$\Delta H_f°(298)$	*R*(CX)	∠CXC	∠XC(HH)	∠(CC)XH
10, X = CH_2	−118.26316	−118.67396	−24.8	1.542	111.6	125.4	126.4 (107.2)[e]
11, X = NH	−134.23515	−134.67565	−4.7	1.485	111.3	128.4	121.3
12, X = O	−154.06177	−154.51480	−44.0	1.433	109.4	128.7	
13, X = CH^-	−117.53823	−117.95158		1.569	105.2	132.9	111.1
14, X = NH_2^+	−134.61049	−135.04860	138.0	1.524	114.1	123.3	126.7 (106.5)[e]
15, X = OH^+	−154.38010	−154.82563	130.1	1.475	118.6	123.1	138.2
16, X = F^+	−178.32647	−178.75831		1.464	119.2	121.5	

[a] Energies in hartree, enthalpies in kcal/mol, bond lengths in Å, angles in deg. In angle notations, (AA) denotes the midpoint between atoms A. [b] HF/A geometries are used. For **1–8** geometries have been recalculated at the HF/C level. Accordingly HF/C//C energies are given. [c] The CH_2 groups are rotated by 3.1° for **2**, 4° for **4**, and 4.2° for **6**. [d] Heats of formation (kcal/mol) from ref 40. [e] ∠HXH angle.

to derive a unified model of 3MRs from the two different MO descriptions by making reference to a quantity which is invariant under unitary transformations of MOs. Such a quantity is the one-electron density distribution $\rho(r)$. Since $\rho(r)$ is an observable upon which other molecular properties depend,[8] it is natural to base a unified model of bonding and electronic structure of 3MRs on the properties of $\rho(r)$.

In this paper, we present a continuation of previous work aimed at an appropriate translation of MO language into an "electron density language".[9-12] Our efforts have been triggered by the topological analysis of $\rho(r)$ developed by Bader and co-workers.[13] It has been shown that investigation of $\rho(r)$ can yield information and draw attention to effects which are difficult to appreciate by examination of a cumbersome set of numbers, either expansion coefficients or overlap populations, which increase with the second power of the number of basis functions.

We will begin by establishing the scenario of a description of 3MRs in terms of the properties of $\rho(r)$ and its associated Laplace field, $\nabla^2\rho(r)$. For this purpose we report results of ab initio calculations on the compounds shown in Chart I. They have been selected in order to show the relationship between 3MRs, charge transfer complexes and alicyclic compounds containing the same heavy atoms. We will draw a connection between these different structures by analyzing their electron density patterns with the aid of catastrophe theory. Then, we will focus on an investigation of bonding in 3MRs with special emphasis on the factors determining their stability, namely ring strain and surface delocalization of σ-electrons. Finally, an account of the chemical relevance of our analysis is given.

While in this paper frequent reference to MO theory is made in order to point out the connection between specific density patterns and the form of the MOs, in the following paper[14] a model of 3MRs is developed which is completely based on the properties of $\rho(r)$, in particular its tendency of concentrating in certain regions of the molecule. The usefulness of this model will be tested for substituted cyclopropanes.

Chart I

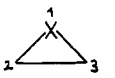

1, X = CH_2
2, X = NH
3, X = O
4, X = CH^-
5, X = NH_2^+
6, X = OH^+
7, X = F^+
8, X = H^+

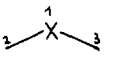

10, X = CH_2
11, X = NH
12, X = O
13, X = CH^-
14, X = NH_2^+
15, X = OH^+
16, X = F^+

$CH_2 = CH_2$

9

CH_3^- (17) $CH_3CH_2^-$ (21) $CH_3CH_2CH_2^-$ (25)
NH_4^+ (18) $CH_3NH_3^+$ (22) $CH_3CH_2NH_3^+$ (26)
OH_3^+ (19) $CH_3OH_2^+$ (23) $CH_3CH_2OH_2^+$ (27)
FH_2^+ (20) CH_3FH^+ (24) $CH_3CH_2FH^+$ (28)

29

30

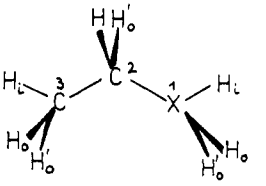

II. Analysis of Energy and Electron Density

Calculations have been carried out at the Hartree–Fock (HF) level of theory employing three different basis sets A, B, and C which correspond to Pople's STO-3G, 4-31G, and 6-31G* bases.[15] Geometries of compounds **1–8** have been optimized at the HF/A and HF/C level while those of the reference compounds **10–28** (Chart I) have only been calculated with basis A.[16]

(8) According to Hohenberg and Kohn (Hohenberg, P.; Kohn, W. *Phys. Rev.* **1964**, *136*, B864–B871) there exists an as yet unknown connection between energy and electron density.

(9) Bader, R. F. W.; Slee, T. S.; Cremer, D.; Kraka, E. *J. Am. Chem. Soc.* **1983**, *105*, 5061–5068.

(10) Cremer, D.; Kraka, E.; Slee, T. S.; Bader, R. F. W.; Lau, C. D. H.; Nguyen-Dang, T. T.; MacDougall, P. J. *J. Am. Chem. Soc.* **1983**, *105*, 5069–5075.

(11) Cremer, D.; Kraka, E. In "Conceptual Approaches in Quantum Chemistry—Models and Applications": *Croat. Chem. Acta* **1984**, *57*, 1265–1287.

(12) Cremer, D.; Kraka, E. *Angew. Chem.* **1984**, *96*, 612–613; *Angew. Chem., Int. Ed. Engl.* **1984**, *23*, 627–628.

(13) (a) Bader, R. F. W.; Nguyen-Dang, T. T.; Tal, Y. *Rep. Prog. Phys.* **1981**, *44*, 893–948. (b) Bader, R. F. W.; Nguyen-Dang, T. T. *Adv. Quantum Chem.* **1981**, *14*, 63–124.

(14) Cremer, D.; Kraka, E. *J. Am. Chem. Soc.*, following paper in this issue.

(15) STO-3G: Hehre, W. J.; Stewart, R. F.; Pople, J. A. *J. Chem. Phys.* **1969**, *51*, 2657–2664. 4-31G: Ditchfield, R.; Hehre, W. J.; Pople, J. A. *J. Chem. Phys.* **1971**, *54*, 724–728. 6-31G*: Hariharan, P. C.; Pople, J. A. *Theor. Chim. Acta* **1973**, 213–222.

Table II. Critical (Stationary) Points of $\rho(r)$

point r_s	(rank,signature)	eigenvalues ($\lambda^1 \le \lambda^2 \le \lambda^3$)	description[a]	associated element	chemical relevance
r_a	(3,−3)	$\lambda^1, \lambda^2, \lambda^3 < 0$	maximum: 3-dim. attractor	basin Ω_A	nucleus
r_b	(3,−1)	$\lambda^1, \lambda^2 < 0, \lambda^3 > 0$	saddle point: 2-dim. attractor	surface S(A,B)	MED path (bond)
r_r	(3,+1)	$\lambda^1 < 0, \lambda^2, \lambda^3 > 0$	saddle point: 1-dim. attractor	edge of at least 3 surfaces	ring structure
r_c	(3,+3)	$\lambda^1, \lambda^2, \lambda^3 > 0$	minimum: repeller	corner of at least 6 surfaces	cage structure

[a] An attractor "attracts" all gradient paths in a volume, in a surface, or along a line.[13]

Table III. Definition of Parameters Used to Analyze Energy and Electron Density

parameter	description (units)
	A. Density Parameters
$\rho_{b,i}$, ρ_r	electron density (e·Å^{-3}) at bond critical point r_b of bond i or at ring critical point r_r
η	ratio $(\rho_r/\bar{\rho}_b)100$ where $\bar{\rho}_b$ is the average of the ρ_b values
n_i	bond order $n = \exp\{a(\rho_{b,i} - b)\}$ of bond i[a]
$\lambda^j_{b,i}$, λ^j_r	principal curvature (eigenvalue of **M**) λ^j (e·Å^{-5}) of ρ at r_b of bond i or at r_r ($\lambda^1 \le \lambda^2 \le \lambda^3$)
v^j	eigenvector of **M** defining direction of principal curvature λ^j
M	Hessian matrix of ρ (matrix of 2nd derivatives)
$\epsilon_{b,i}$	ellipticity (anisotropy) of $\rho_{b,i}$: $\epsilon_b = (\lambda^1/\lambda^2) - 1$[b] ($\lambda^1$ and λ^2 are principal curvatures perpendicular to bond path; $\lambda^1 \le \lambda^2 < 0$; λ^2 is called the soft curvature, its direction given by v^2 is called the major axis of ϵ (π-direction))
ϵ_r	ellipticity (anisotropy) of ρ_r: $\epsilon_r = (\lambda^2/\lambda^3) - 1$ (λ^2 and λ^3 are principal curvatures in the ring plane; $\lambda^3 \ge \lambda^2 > 0$)
$-\nabla^2\rho_{b,i}$, $-\nabla^2\rho_r$	Laplace concentration (e·Å^{-5}) of $\rho_{b,i}$ or ρ_r
$H_{b,i}$, H_r	local energy density (hartree·Å^{-3}) at r_b of bond i or at r_r: $H = G + V$
	B. Geometrical Parameters
r_b, r_r	location of bond critical (3,−1) and ring critical (3,+1) point of $\rho(r)$
l^{ij}_i	location of (3,−3) critical points of $-\nabla^2\rho(r)$ in valence sphere of atom i in the direction of bond i,j
l^{jk}_i	location of (3,−1) and (3,+1) critical points of $-\nabla^2\rho(r)$ in valence sphere of atom i between bonds i,j and i,k
R_i	length of bond i as measured by internuclear distance (Å)
$R_{b,i}$	length of bond path i (Å)
$d_{b,i}$	distance between $r_{b,i}$ and internuclear axis i (Å); negative values indicate that r_b lies inside the geometrical ring
Q_i	ratio $(R_{b,i}/R_i - 1)1000$
p^{ij}_i	distance (Å) of critical point l^{ij}_i of $-\nabla^2\rho(r)$ from the nucleus i
α_i	geometrical angle (deg) at atom i
β_i	interpath angle (deg) at atom i
$\Delta\beta^{ij}_i$	angle (deg) between internuclear axis and bond path from atom i to j
$\gamma_i = \gamma^{jk}_i$	angle (deg) between lines connecting atom i with its charge concentration maxima at l^{ij}_i and at l^{jk}_i
$\Delta\gamma^{ij}_i$	angle (deg) between internuclear axis and vector pointing to concentration maxima at l^{ij}_i

[a] Reference 9. Constants a and b have been taken from ref 11. [b] Reference 9.

In order to obtain a reliable account of the stability of compounds **1–7**, energy calculations have been repeated at a correlation corrected level of theory with second order Møller–Plesset (MP) Rayleigh–Schrödinger pertubation theory.[17] All relevant energies and geometries thus obtained are summarized in Table I. (A full account of calculated energies and geometries is given in the supplementary material.)

The analysis of the one-electron density distribution $\rho(r)$ has been based on an investigation of its critical points r_s, which are the sources and sinks of the gradient paths (trajectories) of the gradient vector field $\nabla\rho(r)$.[13] It is convenient to characterize the critical points r_s by rank and signature of the Hessian matrix **M** of $\rho(r)$.[18] The corresponding notation for rank 3 critical points normally found in a molecule, their characterization, and their chemical relevance is given in Table II.

Of particular interest are the properties of $\rho(r)$ at the (3,-1) critical points r_b in the internuclear region of two interacting atoms. The point r_b is the sink of all gradient paths which define the "zero-flux" surface S(A,B) between two adjacent atoms A and B.[19] At the same time it is the source of two gradient paths determining the line of maximum electron density (MED) between the nuclei of A and B.[20] It is important to note that a MED path does not necessarily coincide with the internuclear axis A–B and, hence, $R_b \ge R_e$ (for a definition of parameters see Table III).

A MED path can be found between any pair of interacting atoms, no matter whether interactions are very weak (e.g., van der Waals interactions, hydrogen bonds, etc.) or very strong (e.g., covalent bonds). In order to distinguish between covalent bonds and closed-shell interactions we have recently analyzed the behavior of the energy density $H(r)$ in the bond regions of a molecule[11]

$$H(r) = G(r) + V(r) \tag{1}$$

where $G(r)$ and $V(r)$ correspond to a local kinetic energy density and the local potential energy density.[21] Since $V(r)$ is always negative and $G(r)$ always positive, the sign of the energy density $H(r)$ reveals whether accumulation of electron density at a point r is stabilizing ($H(r) < 0$) or destabilizing ($H(r) > 0$). Investigation of a variety of different bonds suggests that a negative energy density at r_b is typical for a covalent bond while $H(r_b) \equiv H_b > 0$ is indicative for closed-shell interactions.[11] In addition, the behavior of $H(r)$ in the bonding region can be used as a measure for the type and strength of a covalent bond.[22]

On the basis of these observations we have suggested that the definition of a covalent bond is based on two conditions,[11] namely (1) the existence of a (3,-1) critical point r_b and its associated MED

(16) Where possible basis A geometries have been taken from the literature. **1–3**: ref 1d. **7**: Hehre, W. J.; Hiberty, P. C. *J. Am. Chem. Soc.* **1974**, *96*, 2665–2677. **8**, **17–24**: Lathan, W. A.; Curtiss, L. A.; Hehre, W. J.; Lisle, J. B.; Pople, J. A. *Prog. Phys. Org. Chem.* **1974**, *2*, 175–261. For related studies on **3**, **4**, and **6** see: Hess, B. A., Jr.; Schaad, L. J.; Polavarapu, P. L. *J. Am. Chem. Soc.* **1984**, *106*, 4348–4352. Clark, T.; Chandrasekhar, J.; Spitznagel, G. W.; Schleyer, P. v. R. *J. Comput. Chem.* **1983**, *4*, 294–301. Nobes, R. H.; Rodwell, W. R.; Bouma, W. J.; Radom, L. *J. Am. Chem. Soc.* **1981**, *103*, 1913–1922.

(17) (a) Møller, C.; Plesset, M. S. *Phys. Rev.* **1934**, *46*, 618–622. (b) Pople, J. A.; Binkley, S.; Seeger, R. *Int. J. Quantum Chem. Symp.* **1976**, *10*, 1–19.

(18) Collard, K.; Hall, G. G. *Int. J. Quantum Chem.* **1977**, *12*, 623–637.

(19) For all points of S(A,B) the flux of $\nabla\rho(r)$ vanishes: $\nabla\rho(r)n(r) = 0$ $\forall\, r \in S(r)$. For more details see ref 13.

(20) Bader[13] uses the term "bond path" for any MED path resulting from interactions between atoms. Since we want to distinguish between the various atom,atom interactions, the term "bond path" is used in this work only for covalent bonds.[11]

(21) $G(r) = 1/2\nabla\nabla'\Gamma^1(r,r')|_{r=r'}$; $V(r) = \text{trace}\overleftrightarrow{\sigma}(r)$; $\overleftrightarrow{\sigma}(r) = {}^1/_4(\nabla\nabla + \nabla'\nabla') - (\nabla\nabla' + \nabla'\nabla)\Gamma^1(r,r')|_{r=r'}$; where $\Gamma^1(r,r')$ defines the first-order density matrix. See ref 13.

(22) Integration of $H(r)$ over the interatomic (zero flux) surface S(A,B) leads to values H(A,B) which correlate with bond dissociation energies. Kraka, E.; Cremer, D., to be published.

Table IV. Energy and Electron Density Properties of the CC Bonds in Cyclopropane as Obtained with Different Basis Sets[a]

basis//geometry	ρ_b	n	H_b	$\nabla^2\rho_b$	d_b	R_b	β	γ	ϵ_b
A//A	1.630	1.00	−1.555	−14.77	0.096	1.529	91.9	89.9	0.11
B//B	1.497	0.98	−1.099	−8.10	0.068	1.511	77.8	92.2	0.26
C//A	1.667	0.97	−1.442	−12.67	0.061	1.512	79.0	91.8	0.48
C//B	1.655	0.99	−1.439	−12.63	0.060	1.512	78.9	91.8	0.48
C//C	1.681	0.98	−1.465	−12.86	0.060	1.507	78.8	91.8	0.49

[a] For definition and dimension of parameters see Table III.

Table V. Properties of Energy and Electron Density of Compounds **1**–**9**[a]

parameter	**1** X = CH_2	**2**[b] X = NH	**3** X = O	**4**[b] X = CH^-	**5** X = NH_2^+	**6**[b] X = OH^+	**7** X = F^+	**8**[c] X = H^+	**9** ethylene
$\rho_{b,1}$	1.681	1.823	1.771	1.529	1.533	1.342	1.149	1.211	
$\rho_{b,2}$		1.763	1.819	1.640	1.871	1.966	2.025	2.243	2.448
n_1	0.98	0.97	1.00	0.85	0.77	0.77			
n_2		1.06	1.12	0.94	1.18	1.29	1.36	1.68	2.00
$\nabla^2\rho_{b,1}$	−12.86	−17.79	−1.88	−10.37	−6.28	1.52	9.97	−3.60	
$\nabla^2\rho_{b,2}$		−14.69	−16.05	−12.07	−17.83	−20.49	−22.44	−24.72	−28.65
$H_{b,1}$	−1.465	−2.351	−2.657	−1.398	−2.037	−1.189	−0.522	−0.668	
$H_{b,2}$		−1.609	−1.712	−1.400	−1.779	−1.932	−2.015	−2.478	−2.942
Q_1[d]	6.7	4.1	2.1	6.6	12.8	122.8	350.3		
Q_2[d]		10.9	15.8	4.0	11.6	12.4	10.4	5.1	0
d_1	0.060	0.043	0.004	0.053	−0.038	−0.171	−0.455		
d_2		0.080	0.094	0.052	0.083	0.087	0.083	0.050	0
α_1	60	60.9	62.4	59.1	58.8	57.7	56.2	63.4	
α_2		59.5	58.8	60.4	60.6	61.1	61.9	58.3	
β_1	78.8	76.4	75.8	69.6	77.3	56.7	4.3	0	
$\Delta\beta_1^{12}$	9.4	8.9	6.7	6.5	9.2	−5.7	−26.0	−31.7	
β_2		77.3	72.8	80.2	60.9	19.9	0.02	0	
$\Delta\beta_2^{21}$		5.9	0.2	11.7	−11.8	−53.4	−73.1	−66.6	

[a] Definition and dimension of parameters are given in Table III. C/HF//C calculations. [b] Bond paths leave the plane of the 3MR; projected in-plane angles $\Delta\beta_l^{ij}$ differ only slightly from out-of-plane angles $\Delta\beta_l^{ij}$. [c] T structure. [d] R_b values can be calculated from $(Q/1000 + 1)R$, where R corresponds to the calculated bond length given in Table I.

path linking the nuclei in question (necessary condition) and (2) a negative value of the energy density $H(r)$ at the point r_b (sufficient condition). If condition 2 is fulfilled, we call the MED path a "bond path".[20] Then, the properties of $\rho(r_b) \equiv \rho_b$ can be used to characterize the bond, e.g., its value to obtain the bond order n or its anisotropy ϵ to determine the π-character of the bond[9,10] (see Table III).

It is useful to know where electron density is concentrated or depleted in a molecule. Usually, this is investigated by determining the difference density distribution $\Delta\rho(r)$. From a theoretical point of view the use of $\Delta\rho(r)$ is problematic since it requires the definition of an appropriate reference density $\rho'(r)$ which is difficult to define in many cases.[23] In order to avoid any ambiguities resulting from the need of a reference density, we investigate the Laplace field $\nabla^2\rho(r)$, which is indicative of concentration and depletion of electron density.[24,25] Laplace concentrations provide a description of the valence sphere of a bonded atom. Its (3,-3) critical points l (Table III) can be assigned, on the basis of simple concepts, to bonding and nonbonding electrons.[25] However, it is important to note that the existence of a chemical bond does not necessarily imply a concentration of charge in the internuclear region. For bonds between strongly electronegative atoms, $\nabla^2\rho(r) > 0$ is found in the whole bonding region, in particular $\nabla^2\rho_b > 0$.[12]

In Table III all density quantities and geometrical parameters used in this work are summarized and briefly explained. (See also Figure 4; for a detailed description the reader should consult the original literature.[9-13]) Figure 1 depicts calculated MED paths and Laplace concentrations $\nabla^2\rho(r)$ for some selected 3MRs.

III. Relationship of 3MRs to Alicyclic Systems

In order to set a basis for a better understanding of the chemical properties of 3MRs, we will discuss in the following the various electron density patterns which may result from the interactions of a molecule A_2 with an atom or atomic group X. For a given geometry R of A_2X the corresponding distribution $\rho(r,R)$ is characterized by its molecular graph, i.e., by the critical points and the associated network of MED paths linking the nuclei of a molecule.[13] All points R in nuclear configuration space, i.e., all geometries, with equivalent molecular graphs fill a structural region (see Appendix). A transition from one structural region to another is associated by a discontinuous change in the molecular graph and can be described by catastrophe theory.[26-28]

Investigation of the molecular graphs of A_2X leads to three structural regions I, II, and III shown in the structure diagram of Figure 2a (for a more detailed description, in particular of axes u, v, w, see the Appendix). In this diagram, regions IV–VII comprise the positions of molecular graphs on the boundaries of I–III. The A_2X structures corresponding to one of these regions are best understood by considering relevant orbital interactions for the C_{2v} symmetrical approach of X toward A_2.

Either X or A_2 may possess a low-lying acceptor orbital which can obtain electron density from an appropriate donor orbital of the other group (atom). Donor–acceptor interactions will be largest for orbitals of a_1 symmetry (Figure 3). Then, electron density is built up along the C_2 axis of the system A_2X leading to a molecular graph with T form (Figures 2a and 3a, see also Appendix). Such a molecular graph is found, e.g., for olefin π-complexes whereas the basal A_2 unit with its occupied $\pi(a_1)$

(23) Difficulties arise, e.g., in the case of cations or anions of cyclopolyenes with delocalized charge.

(24) This becomes obvious when considering the definition of the second derivative of ρ in the one-dimensional case:

$$\lim_{\Delta x \to 0} \{\rho(x) - \tfrac{1}{2}[\rho(x - \Delta x) + \rho(x + \Delta x)]\} =$$

$$-\tfrac{1}{2} \lim_{\Delta x \to 0} \{[\rho(x + \Delta x) - \rho(x)] - [\rho(x) - \rho(x - \Delta x)]\} = -\tfrac{1}{2}(d^2\rho/dx^2)\, dx^2$$

If the second derivative is negative, $\rho(x)$ is larger than the average value of ρ at all neighboring points: Morse, P. M.; Feshbach, H. "Methods of Theoretical Physics"; McGraw-Hill: New York, 1953; Vol. 1, p 6.

(25) Bader, R. F. W.; MacDougall, P. J.; Lau, C. D. H. *J. Am. Chem. Soc.* **1984**, *106*, 1594–1605.

(26) Thom, R. "Structural Stability and Morphogenesis"; W. A. Benjamin Inc.: Reading, MA, 1975.

(27) Poston, T.; Stewart, I. "Catastrophe Theory and its Applications"; Pitma: Boston, 1981.

(28) (a) Bader, R. F. W.; Nguyen-Dang, T. T.; Tal, Y. *J. Chem. Phys.* **1979**, *70*, 4316–4329. (b) Bader, R. F. W.; Tal, Y.; Anderson, S. G., Nguyen-Dang, T. T. *Isr. J. Chem.* **1980**, *19*, 8–29.

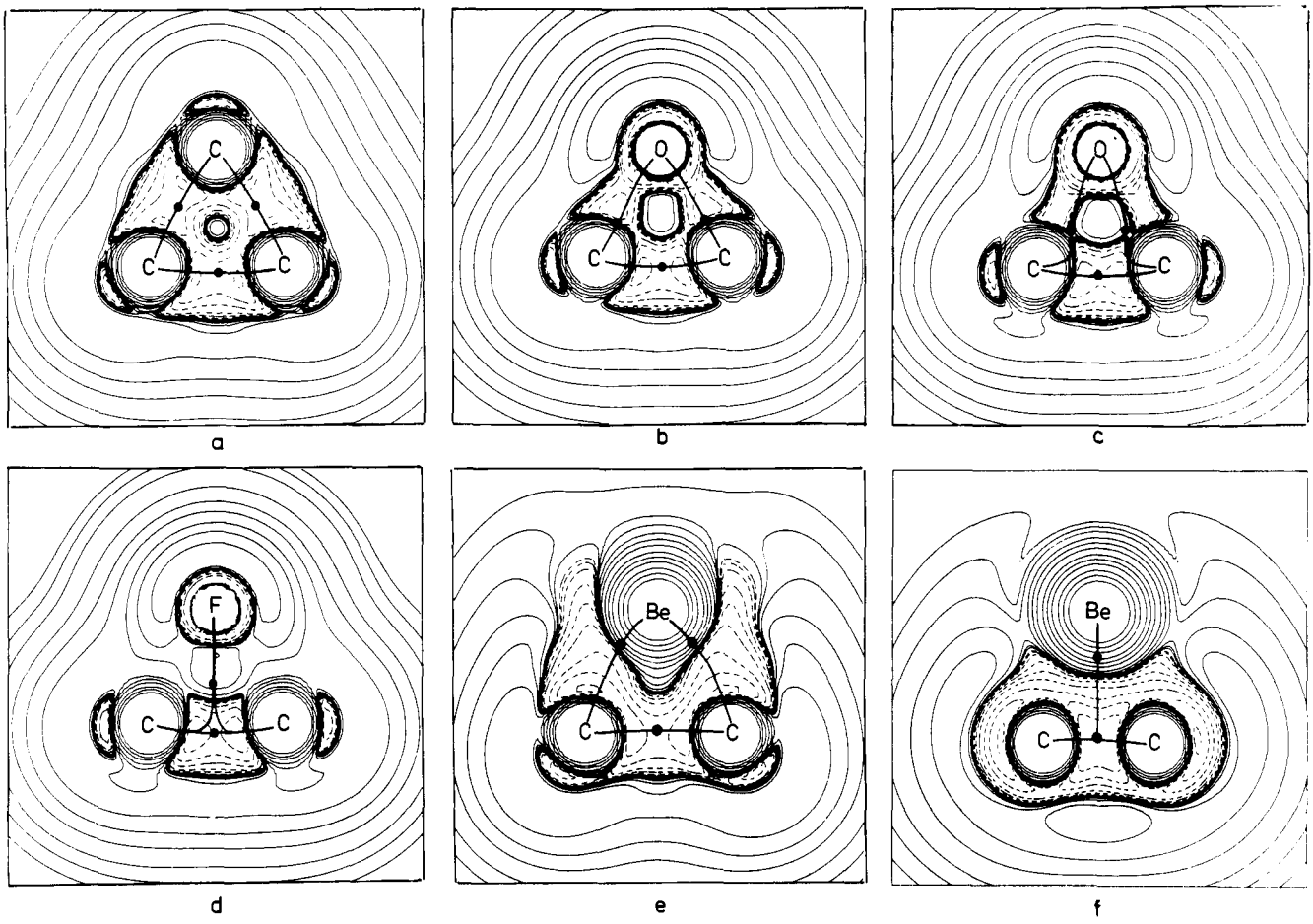

Figure 1. Molecular graphs and Laplace concentrations, $\nabla^2\rho(r)$, of cyclopropane (a), oxirane (b), protonated oxirane (c), halogen-bridged fluoroethyl cation (d), beryllocyclopropane (e), and beryllocyclopropine (f). Bond paths are indicated by heavy lines and bond critical points by dots. Dashed lines are in regions where electronic charge is concentrated ($\nabla^2\rho(\mathbf{r}) < 0$) and solid lines in regions where charge is depleted ($\nabla^2\rho(\mathbf{r}) > 0$). HF/C//C calculations.

MO acts as the donor (Figure 3a). As an example, the density properties of the nonclassical, π-bonded ethyl cation (**8**) are given in Table V. A T form is also found for a system like C_2Be[29] (Figures 1f and 3b). There, the C_2 unit possesses an empty a_1 MO which is C,C-bonding but predominantly nonbonding (lone pair (1p) MO, Figure 3b). By accepting density from the 2s(Be) orbital the C_2 unit is linked with Be by a single bond path ($H_b < 0$).[29]

In T structures with X being the acceptor the bond order of A_2 is diminished by partial depopulation of its a_1 MO. In this way, atoms A become more prone to nucleophilic attack. The reverse is true in T structures with X being the donor. T structures are labile to B_2 displacements of X which lead to an alicyclic molecular graph AAX (Figure 2a, region III). In this case electron density is shifted into the internuclear region between X and one of the groups (atoms) A to yield a stronger A,X bonding interaction. Such a switch in molecular structure is experienced if an olefin π-complex changes to a σ-complex.

If X possesses a high-lying occupied b_2 orbital and the basal group A_2 an appropriate acceptor orbital, interactions between a_1 orbitals will be complemented by those between b_2 orbitals in the same measure as overlap increases for decreasing v. Electronic charge is back-donated via the b_2 MOs, thus leading to a buildup of electron charge along the lines AX. Together with the accumulation of ρ along the C_2 axis resulting from a_1 interactions a plateau of relatively high electron density is formed between A_2 and X. Depending on the electronic nature of X and A or more specifically the energy gap between the b_2 MOs and, hence, the amount of electron charge back-donated, MED paths are formed between A and X. Back-donation increases the electronegativity of X. Accordingly, more density is pulled along the C_2 axis toward X thus leading to a further weakening of the A,A bond. In MO language (Walsh model) these observations are explained by a transfer of electronic charge into the antibonding (b_2) acceptor MO of A_2.

Back-donation and the peripheral buildup of charge associated with it eventually lead to 3MR structures located in region I of Figure 2a. Judging by the appearance of the molecular graphs one can distinguish two types of 3MRs, namely convex-shaped 3MRs with outwardly curved MED paths and concave-shaped 3MRs with inwardly curved MED paths. The former are the result of prevailing back-donation via the b_2 MOs with no or only moderate donation from A_2 to X via the a_1 MOs (Figure 3c). An appropriate example would be the system BeC_2H_4 (Figure 1e), where contrary to the situation in BeC_2 (Figure 1f) donation from 2s(Be) to the C_2 unit is no longer possible since all low-lying a_1 MOs of C_2 are occupied. Concave-shaped 3MRs are encountered if X is more electronegative than A and, accordingly, possesses a relatively low-lying b_2 orbital. In this case, back-donation is moderate leading to an electron density pattern (molecular graph) close to that of the T structures (Figue 3d). The electron density features of **7** (Table V and Figure 1d) suggest that olefin π-complexes with halogenium ions traverse such a 3MR form before rearranging to a σ-complex with the alicyclic XAA^+ structure.

For a three-particle system A_2X the control space $W(u,v,w)$ (see Appendix) has the same dimension as the nuclear configuration space R ($W \subset R$). The structure diagram of Figure 2a has been obtained for a fixed value of the third control parameter $w > 0$. If w approaches 0 the area of the hypocycloid-shaped region I decreases and, eventually, degenerates at the origin of the control space ($u,v,w = 0$) to a single point[28] as is shown in

(29) Schleyer, P. v. R.; Frenking, W.; Gauss, J.; Cremer, D., to be published.

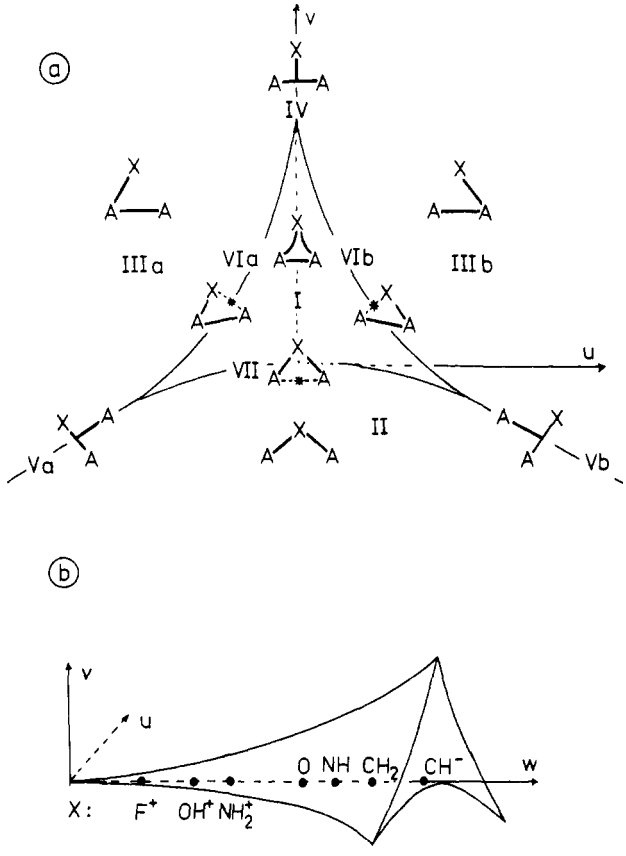

Figure 2. Structure diagram of system A_2X shown in (u, v, w) space. (a) Control parameter w = constant. For each of the structural regions I–VII a molecular graph is given. Asterisks denote catastrophe points. (b) Three-dimensional display of the bifurcation set of the elliptic umbilic in (u, v, w) space for $w \geq 0$ (see Appendix, Table VIII). The meaning of w as a chemical control parameter is illustrated by giving the approximate positions of 3MRs **1**–**7** on the positive w axis.

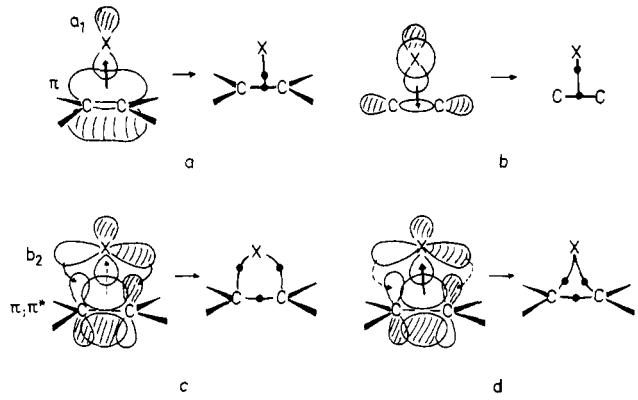

Figure 3. Donor–acceptor interactions between A_2 (C_2H_4 or C_2) and X. The relevant orbitals (a_1 or b_2 symmetry) are shown on the left-hand side and the corresponding molecular graph on the right-hand side of each diagram. The direction of charge transfer is indicated by arrows (dashed arrows indicate reduced charge transfer); dots denote bond critical points. (a) T structure of an ethylene π-complex; (b) T structure of BeC_2; (c) convex-shaped 3MR; (d) concave-shaped 3MR.

Figure 2b. The parameter w leads to a distinction between various systems A_2X and, therefore, can be considered as a chemical control parameter reflecting the electronic nature of both A and X. From the discussion presented above the structural region I decreases the more electronegative X is as compared to A. Therefore, we tentatively relate w to the electronegativity difference between A and X (for A,X not equal H[30]). On this basis,

(30) Although there is a small electronegativity difference between C and H, H does not possess occupied b_2 donor orbitals necessary to form a 3MR.

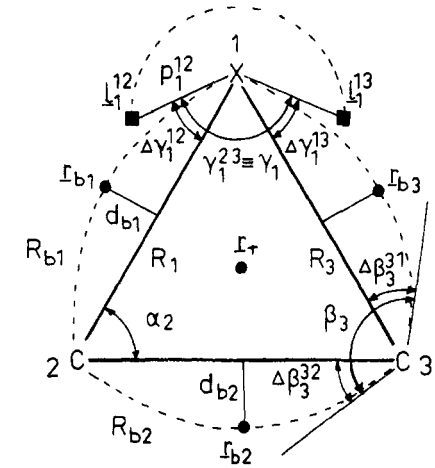

Figure 4. Geometrical parameters used for the description of critical points of $\rho(r)$ (r_b; r_τ) and $-\nabla^2\rho(r)$ (l_i^{ij}). Compare with Table III. Bond paths are indicated by dashed lines. The semicircle around **1** symbolizes part of the valence sphere of **1**.

compounds **1**–**7** investigated in this work can be qualitatively ordered along the positive w axis of the structure diagram as shown in Figure 2b. We will test this assumption in the following sections by analyzing the molecular graphs of **1**–**7** in detail.

IV. Description of Bent Bonds

In VB theory, the bend of a bond is described by the interorbital angle between hybrid orbitals of the type sp^n.[31] For example, the Coulson–Moffit model of **1** describes CC bonding in terms of an overlap of sp^5 hybrid orbitals.[2] Interorbital angles of 102–116°[1e,2,32,33] are found in this way. X-ray diffraction studies of derivatives of **1**, **2**, and **3** have lead to electron difference density maps which displace $\Delta\rho(r)$ maxima g about 0.32, 0.33, and 0.16 Å outside the internuclear axes, yielding angles ∠gXg of 104° (CCC ref 5b, see also ref 5a), 108° (NCC, ref 5c), and 84° (OCC, ref 5d). On the other hand, the calculated electron density distribution arising from the six electrons in the three occupied Walsh MOs of **1** leads to ∠gCg angles of 82°.[34]

Although some of these angles are similar in magnitude, it has to be stressed that interorbital angles and angles derived from difference or valence electron densities *are not comparable quantities*. In particular, *these angles must not be compared with angles obtained from the analysis of total densities*.

In this work we describe the bend of a 3MR bond by the interpath angles β_i, the increment angles $\Delta\beta_i^{ij}$, the distances $d_{b,i}$ and the ratios Q, which are defined in Table III (see also Figure 4). Angles $\Delta\beta_2^{21}$ and $\Delta\beta_2^{23}$ are only equal in the case of X = CH_2, i.e., for compound **1**. We will use $\Delta\beta_2^{21}$ ($\equiv\Delta\beta_3^{31}$) to characterize the shape of the 3MR, namely convex ($\Delta\beta_2^{21} > 0°$) or concave ($\Delta\beta_2^{21} < 0°$).

Influence of Basis Set and Geometry. Before discussing $\rho(r)$, $\nabla^2\rho(r)$, and $H(r)$ of 3MRs in detail it is necessary to make an assessment of their dependence on basis set and geometry. For this purpose some relevant data are collected in Table IV. The computed density properties of **1** reveal the expected basis set dependency. Since basis A has been designed to provide a reasonable description of the bonding region, it leads to relatively high ρ_b values. A split-valence description such as basis B allows charge to move into the regions around the nuclei thus increasing

(31) Bingel, W. A.; Lüttke, W. *Angew. Chem.* **1981**, *93*, 944–956; *Angew. Chem., Int. Ed. Engl.* **1981**, *20*, 899–911.
(32) Newton, M. D.; Switkes, E.; Lipscomb, W. N. *J. Chem. Phys.* **1970**, *53*, 2645–2657.
(33) (a) Randić, M.; Maksić, Z. *Theor. Chim. Acta* **1965**, *3*, 59–68. (b) Maksić, Z.; Eckert-Maksić, M. *Croat. Chem. Acta* **1970**, *42*, 433–438. (c) Vujisić, L.; Vučković, D. L.; Maksić, Z. B. *J. Mol. Struct. THEOCHEM 106*, 323–332.
(34) Kochanski, E.; Lehn, J. M. *Theor. Chim. Acta* **1969**, *14*, 281–304. The interpath angle determined by the total one-electron density was estimated to be 70° (HF/DZ calculations). An interpath angle of 77°, however, was found with a minimal basis of STFs: Stevens, R. M.; Switkes, E.; Laws, E. A.; Libscomb, W. N. *J. Am. Chem. Soc.* **1971**, *93*, 2603–2609.

Table VI. π-Character of Bonds and Degree of Surface Delocalization for Compounds **1–9**[a]

molecule	ϵ_1	ϵ_2	ϵ_r	λ_r^2	direction[b] of v_r^2	ρ_r	η	$\nabla^2\rho_r$	$\epsilon_r(\nabla^2\rho)$
1, X = CH_2	0.489		0	5.47	no	1.379	82.0	1.56	0
2, X = NH	0.502	0.391	0.574	5.33	∥	1.485	83.1	3.31	0.445
3, X = O	0.879	0.314	1.413	4.78	∥	1.533	85.8	5.53	0.094
4, X = CH^-	0.413	0.576	0.236	4.37	⊥	1.307	83.6	1.74	0.270
5, X = NH_2^+	1.584	0.145	2.188	3.46	∥	1.387	85.0	4.65	0.218
6, X = OH^+	2.156	0.046	7.286	1.82	∥	1.305	86.9	7.77	0.186
7, X = F^+	$>10^2$	0.028	$>10^2$	0.01	∥	1.149	85.6	10.00	3.780
8,[d] X = H^+		0.252			∥	1.211		−3.60	7.632
9, ethylene		0.446							
cyclobutane[c]	0.001		0	6.11	no	0.554	33	9.23	0
benzene	0.231		0	2.15	no	0.141	7	3.98	0

[a] For definition and dimension of parameters see Table III. C/HF//C calculations. [b] Direction of major axis of ϵ_r is either parallel (∥) or perpendicular (⊥) to basal CC axis. [c] Geometry from the following: Cremer, D. *J. Am. Chem. Soc.* **1977**, *99*, 1307–1309. [d] T structure.

Table VII. Stability of 3MRs **1–7** as Determined by Isodesmic Bond Separation Energies (IBSE), Homodesmotic Energies (HSE), Conventional Strain Energies (CSE), and Proton Affinities (PA)[a,b]

energy		**1** X = CH_2	**2** X = NH	**3** X = O	**4** X = CH^-	**5** X = NH_2^+	**6** X = OH^+	**7** X = F^+
IBSE	exptl	−19.7	−14.6	−10.0		−24.3	−22.0	
	C/MP	−22.3	−16.0	−12.3	−12.4	−27.4	−26.3	−28.1
	C/HF	−24.7	−21.9	−19.4	−15.5	−28.9	−30.8	−33.6
HSE	exptl	−26.5	−26.4	−27.5		−32.9	−43.2	
	C/MP	−29.7	−29.5	−30.0	−29.4	−42.5	−45.5	−52.3
	C/HF	−28.0	−29.8	−31.6	−25.9	−40.2	−46.5	−54.7
CSE	exptl	27.6	27.7	26.9				

PA		XH_2	CH_3XH	CH_3CH_2XH	CH_3XCH_3	X △
X = CH^-	exptl	416.6				
	C/MP[c] (corr)	416.6	414.3	409.0	411.6	401.3
	C/MP	458.3	456.0	450.7	453.3	443.0
	C/HF	457.1	456.5	452.4	454.9	445.5
X = NH	exptl	207.0	218.4	217.1	224.8	220.1
	C/MP[c] (corr)	207.0	217.4	220.6	224.2	216.8
	C/MP	216.8	227.2	230.4	234.0	226.6
	C/HF	215.5	226.8	230.6	235.5	231.8
X = O	exptl	173.0	184.9	190.3	193.1	185
	C/MP[c] (corr)	173.0	186.6	190.9	193.6	186.2
	C/MP	174.5	188.1	192.4	195.0	187.7
	C/HF	174.0	189.2	194.2	199.8	193.7

[a] All values in kcal/mol. [b] Experimental values derived from heats of formation given in Table I and ref 40. [c] Corrected C/MP values have been obtained by subtracting differences PA(C/MP) − PA(exp) found for XH_2 from calculated PA(C/MP) values.

electron–nuclear attraction. As a consequence, a low value of ρ_b results. Basis C which contains d-GTFs reverts this trend due to a better description of both bonding and nuclear regions. Similar observations can be made for H_b and $\nabla^2\rho_b$.

It is interesting to note that both basis B and basis C lead to a similar description of the geometrical features of the CC bond paths. For example, the interpath angles are 77.8° (B//B) and 78.8° (C//C). Contrary to these results basis A overestimates the bend of the CC bond by about 7° ($\Delta\beta = 16°$, $\beta = 92°$, Table IV). Obviously, this is a result of the rigidity of a minimal s,p basis like A, which enforces an orthogonal arrangement of the bond paths. We conclude that with increasing flexibility of the basis the interpath angle of **1** decreases, approaching a value close to 79°. It is reasonable to expect a similar trend for interorbital angles which would mean that the minimal basis set angle of 108° is just an upper limit to the true interorbital angle.

On the basis of these results the use of basis C seems to be sufficient for a description of 3MRs. Basis C results hardly differ if A, B, or C bases geometries are employed (Table IV). This allows a reliable analysis of 3MRs at the C//B or C//A level of theory if C geometries are not available.[14]

Convex- and Concave-Shaped 3MRs. In Table V energy and electron density properties of compounds **1–8** calculated at the C//C level of theory are summarized. According to calculated H_b values all compounds but **8** possess a 3MR structure with covalent CX and CC bonds. The values of $H_{b,2}$, $\rho_{b,2}$, n_2, and $\nabla^2\rho_{b,2}$ suggest a continuous increase of the CC bond strength for increasing electronegativity of X, i.e., in the series

$$X = CH^-, CH_2, NH, O, NH_2^+, OH^+, F^+ \qquad (2)$$

It is important to note that the trend in computed R_2 values (Table I) deviates slighlty from that suggested by $H_{b,2}$ and $\rho_{b,2}$. $R_{b,2}$ values, on the other hand, are parallel to $H_{b,2}$ and $\rho_{b,2}$, suggesting that bond path lengths rather than internuclear distances should be used if bond properties of strained systems are correlated with bond length.

The bond orders reveal significant weakening of the CX bonds in the case of the charged 3MRs. This is also reflected by $\rho_{b,1}$, $\nabla^2\rho_{b,1}$, and $H_{b,1}$ although these properties do depend on the atomic numbers of the atoms linked. According to calculated shift parameters $d_{b,i}$ and interpath angles β_i, in particular the increment angles $\Delta\beta_1^{12}$ and $\Delta\beta_2^{21}$, **1–8** can be classified in the following way. Compounds **1**, **2**, and **4** possess convex and compounds **5**, **6**, and **7** concave CX bond paths. 3MR **3** takes an intermediate position and **8** is a true T structure. The bend of the 3MR bonds as measured by Q is actually largest for inwardly curved CX bonds of concave-shaped 3MRs **5**, **6**, and **7**. The bend of the CC bond increases in the series **4**, **1**, **2**, **3** (Table V).

These data confirm that with increasing electronegativity of X the 3MR approaches the T form of an ethylene π-complex (Figure 3a). In series (2) charge is increasingly transferred from the a_1 (π) MO of the CH_2CH_2 unit to X while at the same time X shows decreasing tendency of back-donating electron density via its p (b_2) MO (Figure 3d). This interpretation is supported by features of the Laplacian field $\nabla^2\rho(r)$ which are discussed below.

Description of Bent Bonds in Terms of Concentrations of $\rho(r)$. For an isolated atom with spherically averaged electron density, charge is concentrated in spheres which can be associated with quantum shells.[25] In the valence region of the atom, the value

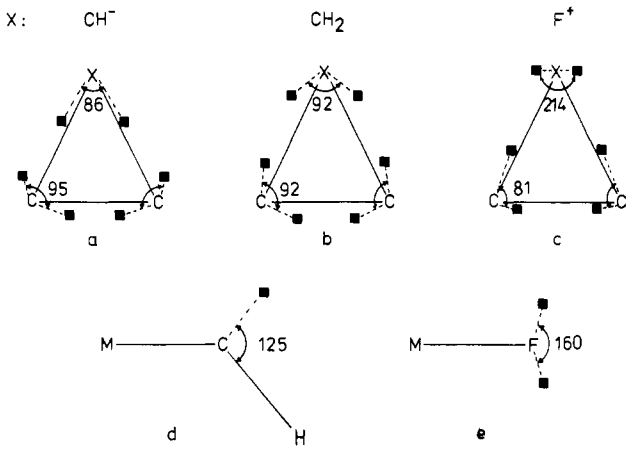

Figure 5. Schematic representation of bonded (a–c) and nonbonded (d, e) concentration maxima (■) in 3 MRs: (a and d) cyclopropylanion; (b) cyclopropane; (c and e) halogen-bridged fluoroethyl cation. Angles γ (a–c) and θ (d, e) are indicated. M denotes the midpoint of the distance C_2C_3.

of $-\nabla^2\rho(r)$ attains a maximum at a radius p_A which defines the radius of the "valence sphere" of the Laplace concentration. The shell structure of $\nabla^2\rho$ for an isolated atom is perturbed upon bonding interactions with other atoms. Local maxima ("lumps") and minima ("holes") emerge in the valence sphere of $\nabla^2\rho$ which can be ascribed to bonded and nonbonded electron pairs.[25]

In an alkane, two bonded C atoms each possess a (3,-3) critical point l_c^{cc} (Table III) of $-\nabla^2\rho(r)$ in their valence spheres. Points l_c^{cc} are located on the internuclear axis at a distance p_c^{cc} from the corresponding nucleus. For cyclopropane, however, concentration maxima l_c^{cc} are substantially displaced from the internuclear connection lines (d_b = 0.143 Å). Hence, at each C atom two geminal concentration maxima l_c^{cc} form an angle γ of 92° rather than 60°.

The locations l_l^{ij} of bonded and nonbonded concentration maxima in the valence spheres of the 3MR atoms of **1–8** depend on the electronegativity of X. With increasing electron acceptor ability of X points l_c^{cc} are pulled toward the C nucleus, while maxima l_c^{cx} are shifted toward X. The valence spheres of the two basal C atoms are distorted by X as is qualitatively shown in Figure 5 (for full details see supplementary material).

Angles γ_2 decrease in series (2) from 95° (**4**) to 81° (**7**) due to the distortion of the valence spheres of the C atoms by X. At the same time the angle γ_1 widens from 86° (**4**) to 214° (**7**). This change in γ_1 is a reminder of the reduced tendency of an electronegative X of back-donating charge into AX bond regions. If this density is completely kept at X it should reside in a b_2 orbital yielding a γ_1 of 180°.

It is interesting to note that the two nonbonded charge concentrations above and below the ring plane of compounds **3** and **7** form large angles θ (156, 160°) with the O and the F nucleus, respectively (see Figure 5). If X possesses only one nonbonded concentration maximum, then the angle θ narrows to 122–125°. The nonbonded charge concentrations are larger and more tightly pulled to the nucleus the more electronegative X is.

V. Ring Strain and Surface Delocalization

Due to its topological features cyclopropane possesses relatively high electron density in the plane of the 3MR. At the minimum of $\rho(r)$ in the ring plane, the value of ρ_r is still 82% of that at the bond critical points (see η in Table VI). In cyclobutane or benzene there is just 33% and 7% of the density at the r_b(CC) points (Table VI). Hence, **1** is unique in the sense that electron density is smeared out all over the ring plane in a similar manner as it is along the CC framework of butadiene or, more pronounced, along that of benzene. Since the density distribution of benzene is a result of *ribbon delocalization* of π-electrons, we describe the density pattern of cyclopropane by the term *surface delocalization* and consider surface delocalization to arise from the (aromatic) delocalization of 6 σ-electrons in the plane of the ring.[35,36] In the following we will discuss those electronic features of a 3MR which may be considered to be related to or to result from surface delocalization of σ-electrons.

π-Character of Cyclopropane Bonds. In Table VI ellipticities ϵ_i obtained for the 3MR bonds of **1–7** are shown. Contrary to normal σ-bonds in hydrocarbons ($\epsilon \approx 0$), all ϵ values are larger than 0, ranging from 0.05 to 0.58 for the bond C_2C_3. The CC bonds of **1** possess an ellipticity (0.49, **1**) exceeding that of benzene (ϵ = 0.23[9]) considerably. Contrary to the anisotropy of an alkene or cyclopolyene double bond, the major axis of ϵ given by the direction of v^2 is not perpendicular but parallel to the plane of the carbon nuclei.[9] This means that in the ring plane the electron density extends both toward the ring center and toward the outside of the ring leading to relatively high η value (Table VI) and to the convex-shaped molecular graph of **1**. The σ-electron density of **1** clearly reveals features of the π-density of an alkene double bond, which complies with the description of the 3MR as a special case of a π-complex. On this basis, the dependency of ϵ_2 on the electronegativity of X (Table VI) is easily understood. The more electronegative X is the more is density in the CC bonding region contracted toward the internuclear CC axis, yielding high values of ρ at r_b. The same features are revealed by the anisotropy of charge concentration at the (3,-1) critical points l^{23} in the CC bond region of **1–7**.

Direction of Surface Delocalization. At the ring critical point r_r of **1**, the two positive curvatures of ρ_r are equal ($\lambda_r^2 = \lambda_r^3$), i.e., the anisotropy of ρ in the ring plane measured by the ellipticity ϵ_r (Table III) is zero and surface delocalization undirected. In an ideal π-complex with T structure, density between H_2CCH_2 and X may be thought of as arising from the two bonding π-electrons of the double bond. In this case the ellipticity of the CC bond is removed (ϵ = 0). A priori it is difficult to assess the magnitude of ϵ at the r_b point of the (A_2)–X bond. But as soon as back-donation from X begins to contribute to bonding, the major axis of this bond has to be parallel to the basal AA axis.

If the CX bonds strengthen at the cost of A,A bond strength, density concentrates in the CX bond region leading to relatively large values of the curvature of ρ parallel to the CC axis. At the same time value and location of ρ_r and ρ_b(CC) approach each other to form finally a (2,0) critical point (see Appendix) equivalent to a loss of the AA bond path (region VII, Figure 2a). Weakening of the AA bond will cause an increase of its ellipticity with the effect that density is pushed into the area of two strong CX bonds.

In conclusion, surface delocalization of 3MRs will be oriented either parallel (concave-shaped 3MR, π-complex) or perpendicular (convex-shaped 3MR, weakening of AA bond) to the basal A,A axis. The direction is measured by the major axis v_r^2 of ϵ_r.

With the exception of **4**, surface delocalization of σ-electrons in **1–7** is always directed parallel to the basal CC bond enhancing the π-character of the CX bonds and reducing that of the CC bond. Both ϵ_r and $\epsilon_1 = \epsilon_3$ are particularly large for compounds **5–7** which again is indicative of their similarity to π-complexes. Only in the case of **4** is surface delocalization perpendicular to the basal CC bond thus enhancing its π-character. These observations are relevant when a 3MR is incorporated into the conjugated chain of a cyclopolyene. From the direction of surface delocalization of the 3MR and the mode of its incorporation into the cyclopolyene it will depend whether ribbon delocalization of π-electrons is sustained in the cyclopolyene (see section VI).

Energetical Consequences of Surface Delocalization: Ring Strain vs. σ-Aromaticity. The angle strain in **1** is calculated, using its geometrical angle of 60° and a CCC bending force constant of 1.07 (mdyn·Å)/rad^2,[37] to be as high as 173 kcal/mol. Considering the anharmonicity in bending as well as eclipsing strain, the actual strain of **1** should be larger than 180 kcal/mol, a value which is

(35) Delocalization of σ-electrons leading to σ-aromaticity has been invoked to explain the conformational behavior of geminal double rotors. Cremer, D.; Binkley, J. S.; Pople, J. A.; Hehre, W. J. *J. Am. Chem. Soc.* **1974**, *96*, 6900–6903.

(36) Dewar, M. J. S. *J. Am. Chem. Soc.* **1984**, *106*, 669–682.

(37) Snyder, R. G.; Zerbi, G. *Spectrochim. Acta* **1967**, *23A*, 391–437.

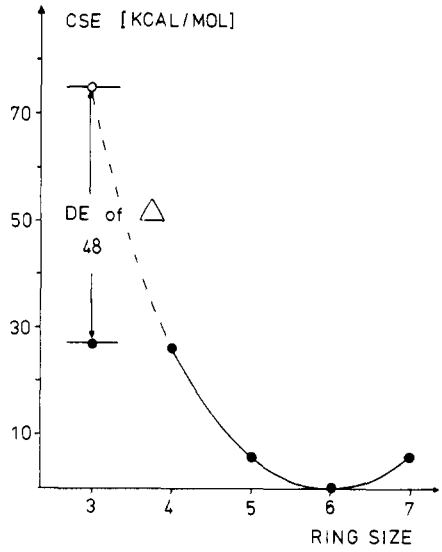

Figure 6. Dependence of conventional strain energies (CSE; ●) of cycloalkanes[41] on the size of the ring. Aromatic delocalization energy (DE) and real strain (○) of cyclopropane are given.

hardly realistic in view of the fact that **1** is a synthesizable compound.

If one considers the MED paths as a result of atom, atom interactions and the geometrical location of the MED paths as the best energetic compromise between stabilizing and destabilizing forces exerted on the electrons, then it seems reasonable to estimate angle strain of 3MRs by utilizing calculated interpath angles β_i rather than geometrical angles α_i (Table V). In this way, angle and total strain of **1** are estimated to be about 66 and 75 kcal/mol. It is interesting to note that a strain energy of this magnitude would be expected for **1** if thermochemically determined conventional strain energies (CSE) of cyclohexane, cyclopentane, and cyclobutane would be extrapolated to that of **1** (see Figure 6).

The actual stability of 3MRs can be evaluated either from isodemic bond separation energies (IBSE, reaction 3) or homodesmotic separation energies[38] (HSE, reaction 4).

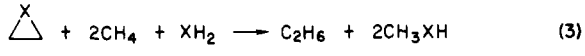

(3)

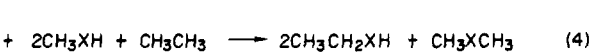

(4)

When using energies and heats of formation, $\Delta H_f°$, of Table I together with relevant data from the literature,[39,40] the IBSE and HSE values of Table VII are obtained. The HSE value of **1** compares well with the corresponding CSE determined from thermochemical group additivity increments[41] (see Table VII). Compared to propane as the appropriate reference compound, **1** is destabilized by 27 kcal/mol, i.e., two-thirds of the estimated strain energy of **1** are compensated by the stabilizing effect of six σ-electrons delocalized in the surface of the ring. The delocalization energy is more than twice as large as that due to ribbon delocalization in benzene (21 kcal/mol[42]). Therefore, *it is justified to consider* **1** *as a* σ*-aromatic system with an aromatic delocalization energy of 48 kcal/mol.*

An independent estimate of the delocalization energy of **1** can be obtained in the following way. The bond,bond interaction energy of the trimethylene biradical ($\Delta H_f° \approx 67$ kcal/mol[43]) is 4 kcal/mol as measured by the formal reaction

$$\dot{C}H_2CH_2\dot{C}H_2 + CH_4 \rightarrow 2CH_3\dot{C}H_2 \qquad (5)$$

The bond,bond interaction energy will attain a maximum value if the terminal CH_2 groups of trimethylene coincide to form ethylene (**9**). Then, the

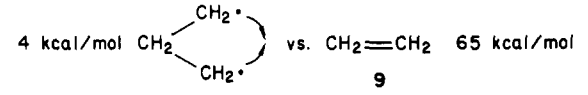

interaction energy (between the "bent bonds" of **9**) has increased to 65 kcal/mol, the contribution of the π-bond to the total CC bond energy of **9**.[41] If a linear increase of the bond,bond interaction energy from trimethylene ($\alpha = 109°$) to ethylene ($\alpha = 0°$) is assumed, then 28% of the 60 kcal/mol gain in energy, i.e., 16.8 kcal/mol, can be attributed to each bond pair of **1** ($\beta = 79°$), thus leading to an overall stabilization by about 50 kcal/mol. Again, this energy is due to σ-aromaticity (surface delocalization) since bond,bond interactions are accompanied by a density buildup in the interbond region as found for **1**.

To which extend do angle strain, σ-aromaticity, and CSE of **1** change if one CH_2 group is replaced by X? To answer this question we will consider convex- and concave-shaped 3MRs separately. Calculated IBSE values (Table VII) increase in the series **1**, **2**, **3**, **4**, which is due to an increase of bond,bond interaction energies also encountered in the appropriate three heavy atom reference compounds (e.g., the experimental IBSE values of **10**–**12** are 2.2, 4.5, and 5.9 kcal/mol). The HSE values, however, are essentially the same for **1**–**4**. Although this might suggest a similarity in strain energies of **1**–**4**, the following observations refute such a conclusion. (a) The CXC and CCX bending force constants increase with the electronegativity of X (e.g., k(COC) = 1.31, k(CCO) = 1.18 (mdyn·Å/rad^2 [37]). The interpath angles β decrease in the series **1**, **2**, **3**, **4** (Table V). Obviously, angle strain is considerably larger for aziridine and oxirane as for **1**. (b) If two CX bonds are held at an angle 30–40° smaller than that in CH_3XCH_3, bond,bond interactions will increase significantly. Accordingly, they cannot be equal on the two sides of the homodesmotic reaction 4. (c) The η values of Table VI indicate an increase of surface delocalization (σ-aromaticity) from **1** to **3**. (d) Due to considerable change in 3MR geometries the variation in bond energies as a function of X may be different on the two sides of reaction 4. In view of (a)–(d) the similarity of HSE values for **1**–**4** is likely to result from cancellation of changes in ring strain, σ-aromaticity, and bond energies.

In the case of the concave-shaped 3MRs, the notion of ring strain as well as that of σ-aromaticity losses its heuristic value. The XC bonds are not fully developed for **5**, **6**, and **7** as is revealed by bond order and $H_{b,l}$ values (Table V). Compounds **5**–**7** as well as **8** are labile: The corresponding IBSE and HSE values are significantly more negative than those of their respective neutral counterparts (Table VII). This becomes even more apparent when the proton affinities of HXH, MeXH, EtXH, and MeXMe are compared with those of the corresponding 3MRs (X = CH^-, NH, O, Table VII[44]). For X = NH and O the proton affinities increase with increasing methylation of X indicative of hyperconjugative stabilization of the protonated systems. This is no longer true

(38) George, P.; Trachtman, M.; Bock, C. W.; Brett, A. M. *Tetrahedron* **1976**, *32*, 317–323.

(39) For HF and MP energies not tabulated in this work, see: Cremer, D. *J. Compt. Chem.* **1982**, *3*, 154–164, 165–177.

(40) For experimental $\Delta H_f°(298)$ and proton affinities, see: (a) Cox, J. D.; Pilcher, G. "Thermochemistry of Organic and Organometallic Compounds"; Academic Press: London, 1970. (b) Bowers, M. T., Ed. "Gas Phase Ion Chemistry"; Academic Press: New York, 1979; Vol. 2. (c) Aue, D. H.; Webb, H. M.; Bowers, M. T. *J. Am. Chem. Soc.* **1975**, *97*, 4137–4139.

(41) Benson, S. W. "Thermochemical Kinetics", 2nd ed.; Wiley: New York, 1976.

(42) George, P.; Trachtman, M.; Bock, C. W.; Brett, A. M. *Theor. Chim. Acta* **1975**, *38*, 121–129.

(43) This value is obtained from the barrier to cis–trans isomerization of 1,2-dideuteriocyclopropane (65 kcal/mol), $\Delta H_f°(298)$ of **1** (12.7 kcal/mol) and the estimated barrier of recycling the trimethylene biradical intermediate (10 kcal/mol). See ref 41, pp 117–128 and the following: Dowd, P.; Chow, M. *J. Am. Chem. Soc.* **1977**, *99*, 6438–6440.

(44) Proton affinities of systems with diffuse lone pairs are overestimated by basis C due to the lack of diffuse s,p GTFs in the basis (see, e.g.: Spitznagel, G. W.; Clark, T.; Chandrasekhar, J.; Schleyer, P. v. R. *J. Compt. Chem.* **1982**, *3*, 363–371). This has been taken into consideration by calibrating calculated proton affinities with experimental values of the parent systems XH_2.

Table VIII. Description of Structural Regions of the A_2X Structure Diagram

structural region	no. of critical points of ρ (3,−3)	(3,−1)	(3,+1)	(2,0)[a]	form of molecular graph	structure of A_2X	catastrophe
I	3	3	1		3M ring	$\overline{A-X-A}$	none
II	3	2			C_{2v} chain	A–X–A	none
IIIa,b	3	2			C_1 chain	A–A–X	none
IV	3	2			C_{2v} T form	(A_2)–X	conflict
Va,b	3	2			C_1 T form	(AX)–A	conflict
VIa,b	3	2		1	change from 3MR to C_1 chain		bifurcation
VII	3	2		1	change from 3MR to C_{2v} chain		bifurcation

[a] Singularity of $\rho(r)$.

for the 3MRs where a decrease of proton affinities (relative to MeXMe) is observed (Table VII). Again, this is indicative of the weakening of the CX bonds and the change from a convex- to a concave-shaped 3MR. The reverse trend is found for X = CH^- (Table VII).

VI. Chemical Relevance of the Analysis of $\sigma(r)$ and $H(r)$

The peculiar chemical properties of **1** (e.g., thermochemical stability (CSE), reactivity in electrophilic addition reactions, barrier of ring opening, upfield shift of signals in ^1H NMR, etc.) have recently been discussed by Dewar on the basis of PMO theory.[36] Dewar's description of **1** as a σ-aromatic system and the conclusions derived therefrom are fully confirmed by our analysis of $\rho(r)$. Therefore, we will refrain from discussing the properties of **1** in more detail. Instead we will demonstrate the chemical implications of surface delocalization for 3MRs in general.

The 3MR as a Conjugate System. The ability of 3MRs to interact with π-systems is easily understood in view of the relatively high ellipticities of their bonds. To ensure conjugation, the major axes of the interacting bonds have to overlap effectively as indicated in **31**.[10] From the discussion of surface delocalization

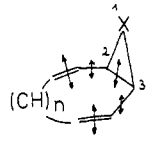

31

in compounds **1–7** some useful conclusions can be drawn. (a) Since electronegative groups X reduce the π-character of the 2,3 bond and thereby π-conjugation in **31**, it is unlikely to observe homoconjugation in a cyclic system containing an aziridine or oxirane ring. An electropositive (donor) group X should lead to the opposite effects and, therefore, should be interesting in studies on homoaromaticity. We will pursue this aspect in more detail in the following paper.[14] (b) An electronegative X strengthens the 2,3 bond which has been verified in many instances. For example, in systems containing the oxirane ring, opening of the 2,3 bond requires more energy than in the corresponding cyclopropane systems.[45] An electropositive X labilizes the 2,3 bond which means that homoconjugative effects can only be observed if the 2,3 bond is clamped together, eventually by a 2,3 bridge as in **32**. (c) The unique properties of 3MRs, in particular those

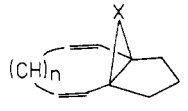

32

of **1**, are lost when extending a 3MR to a 4MR. The calculated distributions $\rho(r)$ and $\nabla^2\rho(r)$ of cyclobutane (Table VI) indicate that both the π-character of the ring bonds and σ-delocalization in the ring surface no longer play a role in the 4MR. Accordingly, it is unlikely to observe homoconjugative effects (homoaromaticity) in cyclopolyenes with a saturated 4MR or two adjacent CH_2 groups incorporated into the conjugative chain.

Reactions of 3MRs with Electrophiles or Nucleophiles. From the concentration pattern of 3MRs shown in Figure 1 and the data collected in Table VI (ϵ_i values) it is obvious that the primary attack at the ring by an electrophile is edge directed. At the early stage of reaction a T structure (π-complex) is formed similar to that expected for alkenes. If the electrophile closes in onto the 3MR, it will move to one of the (3,-3) concentration maxima thus yielding a corner intermediate. In those cases, where X possesses nonbonded charge concentrations (e.g., **2**, **3**, **4**) the electrophile will immediately attack X.

The basal C atoms of **1–7** possess concentration holes in their spheres which are suitable for a nucleophilic attack. As can be seen by inspection of Figure 1, these holes widen and extend more into space as X becomes more electronegative. This has to do with the fact that the basal CH_2 groups bent toward the positions adopted in a free ethylene molecule (see angle ∠CC(HH) in Table I). Hence, nucleophilic attack at concave-shaped 3MRs, i.e., 3MRs structurally related to π-complexes, should be faster than that at convex-shaped 3MRs.

Protic or Lewis acids will increase the reactivity of 3MRs like **1**, **2**, or **3** by converting them to concave-shaped ring structures with labile CX bonds. Small lateral displacements of X from its equilibrium position, caused, e.g., by a nucleophilic attack on the basal C atom, will lead to immediate CX bond rupture. This situation is encountered, e.g., in the acid-catalyzed ring opening reaction of oxiranes (see below). Needless to say the protic or complexing solvents can also lead to rate acceleration in additon reactions.

Reaction of Oxiranes with Nucleophiles. The addition of nucleophiles to oxiranes to form 1,2-disubstituted products is widely used in syntheses.[46] Ring opening is observed in neutral, basic, and acidic solution, but it is known that the presence of acid accelerates the reaction significantly. With an unsymmetrically substituted **3** like **29** (Chart I), nucleophilic attack occurs predominantly at the sterically less hindered C atom in neutral and basic solution while in acid solution the higher substituted C atom of **30** is attacked. Since ring opening is always accompanied by a Walden inversion, the S_N1 mechanism can be ruled out in acid media.[46]

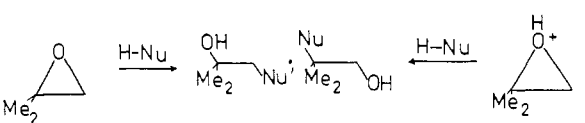

29 (6) 30

In order to rationalize these observations, we have calculated $\rho(r)$, $\nabla^2\rho(r)$, and $H(r)$ for both **29** and **30** at the HF/C level of theory, utilizing basis C geometries of **3** and **6**. The results of our analysis are depicted in Figure 7. According to the properties of ρ and H at the bond critical points $r_{b,1}$ and $r_{b,2}$, there is hardly

(45) (a) Pommelet, J. C.; Cuche, J. *Tetrahedron Lett.* **1974**, 3897–3898. (b) Grimme, W.; Seel, K. *Angew. Chem., Int. Ed. Engl.* **1973**, *12*, 507–508.

(46) (a) Buchanan, J. G.; Sable, H. Z. In "Selective Organic Transformations"; Thyagarajan, B. S., Ed.; Wiley: New York, 1972; Vol. 2, pp 1–95. (b) Smith, J. G. *Synthesis* **1984**, 629–656.

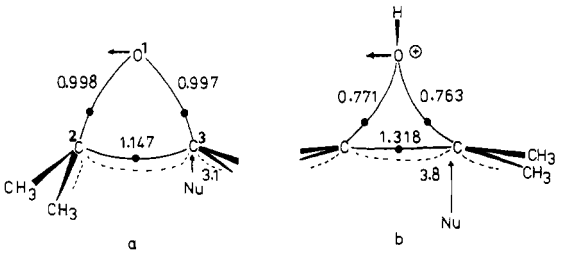

Figure 7. Nucleophilic (Nu) attack at (a) an oxirane (**29**) and (b) a protonated oxirane (**30**). Bond orders from HF/C calculations are depicted. Positions of concentration holes at basal C atoms are indicated by dashed lines. $\nabla^2\rho(r)$ is given at each center of attack. Arrows denote movement of Nu and O, respectively.

any difference between the CO bonds in **29**, both being normal bonds of order 1. For **30**, however, two partial bonds ($n < 1$, but $H < 0$) are found which differ significantly as revealed by ρ_b, $\nabla^2\rho_b$, and H_b values. Bond O_1C_2 is clearly weaker than bond O_1C_3. Any attack of the nucleophile at the basal C atoms will lead to CO bond rupture with a preference for the rupture of the weaker bond. The latter, however, implies an attack at the sterically more hindered basal C atom. This is faciliated in two ways. First, the two methyl groups are bent toward the CO bonds typical for concave-shaped 3MRs (see angles ∠CC(HH) in Table I). As a consequence the concentration holes at C_2 are sterically less shielded in **30** than in **29**. Second, the concentration holes at C_2 of **30** are larger and extend more into space than those at C_2 of **29**. Because of this and the ease of breaking bond O_1C_2 in **30**, a loose contact between nucleophile (Nu) and 3MR at C_2 is energetically sufficient to start the reaction.

In the case of **29**, the strength of the CO bonds requires a close contact between Nu and the basal C atoms which is impeded at C_2 due to the fact that the Me groups shield the concentration holes. Accordingly, nucleophilic attack occurs preferentially at the CH_2 group, yielding the product observed experimentally.[46] It is important to note that this rationalization of the observed regioselectivity of oxirane cleavage does not need to speculate on the charge distribution in the transition state of the reaction.

Acknowledgment. We thank Doz. Dr. H.-J. Altenbach for useful discussions. Support by the Deutsche Forschungsgemeinschaft and the Fonds der Chemischen Industrie is acknowledged. All calculations have been carried out at the Rechenzentrum Köln.

Appendix

Molecuar graphs that possess the same number of MED paths linking the nuclei of a molecule are equivalent.[13] For a given molecular state there exists a finite number of classes of equivalent molecular graphs (structures) and associated regions of nuclear configuration space. Accordingly, the equivalence relation of molecular graphs can be used for the partitioning of nuclear configuration space into structural regions.[28] At the boundaries of the structural regions thus defined a differential change in geometry leads to a discontinuous change in the molecular graph (structure) which can favorably be described by catastrophe theory.[26,27] In terms of this theory such a change in structure is called a catastrophe.[26,27]

In order to apply catastrophe theory to structural changes of a three-particle system A_2X, and appropriate control space W[27] has to be defined. W possesses the same dimension as the nuclear configuration space R of A_2X and is spanned by the control parameters u, v, w. For convenience the molecular graphs of A_2X are first analyzed in a subspace of W, namely the plane defined by axes u and v and located at w = constant of the positive w axis (Figure 2). Control parameters u and v are chosen to describe the two independent coordinates of X. For every (u, v) point the third degree of freedom of A_2X is considered to be optimized. In this way, v gets the meaning of the reaction coordinate of a C_{2v} symmetrical approach (decreasing v) of X toward A_2 (A_1 symmetrical displacement of X) and u describes B_2 symmetrical displacements of X from this reaction path.

As shown in Figure 2a the stable molecular graphs of A_2X belong to one of the three structural regions I, II, and III. The boundaries of the three regions are determined by the set of all catastrophe points which is mathematically described by the unfolding of the elliptic umbilic catastrophe.[26-28] (An unfolding is a family of functions describing a given type of catastrophe completely.) Thus, regions IV and Va,b denote the positions of all conflict catastrophes and regions VIa,b and VII the positions of all bifurcation catastrophes. The features of stable molecular graphs (I–III) as well as catastrophe graphs (IV–VII) are summarized in Table VIII.

Registry No. 1, 75-19-4; **2**, 151-56-4; **3**, 75-21-8; **4**, 1724-45-4; **5**, 24151-28-8; **6**, 27659-85-4; **7**, 53172-39-7; **8**, 25215-44-5.

Supplementary Material Available: Tables of calculated energies and geometries for 3MRs and **10–28** and a description of heavy-atom valence spheres of **1–7** (6 pages). Ordering information is given on any current masthead page.